2017-01

Correcting wave reflection estimates in the coastal zone

Inch, K

http://hdl.handle.net/10026.1/8465

10.1016/j.coastaleng.2016.09.004
Coastal Engineering
Elsevier BV

Elsevier Editorial System(tm) for Coastal Engineering

Manuscript Draft

Manuscript Number: CENG-D-16-00062R1

Title: Correcting Wave Reflection Estimates in the Coastal Zone

Article Type: Research Paper

Keywords: Wave reflection; noise; coherence; linear wave theory

Corresponding Author: Mr. Kris Inch,

Corresponding Author's Institution: University of Plymouth

First Author: Kris Inch

Order of Authors: Kris Inch; Mark Davidson; Gerd Masselink; Paul Russell

Abstract: The impact of random noise on an existing two-dimensional method for separating incident and reflected wave spectra using an array of wave gauges is investigated using simulated time series with known wave amplitudes, reflection coefficients, and signal-to-noise ratios. Both the incident and reflected spectra are overestimated by a quantity that can exceed 100% for signal-to-noise ratios less than 1. Consequently, estimated reflection coefficients are also overestimated with larger errors occurring when the known reflection is low. Coherence decreases systematically with increasing noise and this trend is used to develop a mathematical function to correct for the observed bias and provide 95% confidence intervals for incident and reflected spectra and reflection coefficients. The correction technique is shown to be very effective in reducing error by up to ~90%. Field data from a natural beach are used to demonstrate the application of these results; corrected values suggest that reflection coefficients are frequently overestimated by over 50%.

Correcting Wave Reflection Estimates in the Coastal Zone

Kris Inch*, Mark Davidson, Gerd Masselink and Paul Russell

School of Marine Science and Engineering, Plymouth University, Drake Circus, Plymouth, Devon PL4 8AA. United Kingdom. kris.inch@plymouth.ac.uk, M.Davidson@plymouth.ac.uk, gerd.masselink@plymouth.ac.uk, P.Russell@plymouth.ac.uk

* Corresponding author. Tel.: +44 (0)1752 586100; Fax: +44 (0)1752 586101; Email: kris.inch@plymouth.ac.uk (Kris Inch).

Abstract

The impact of random noise on an existing two-dimensional method for separating incident and reflected wave spectra using an array of wave gauges is investigated using simulated time series with known wave amplitudes, reflection coefficients, and signal-to-noise ratios. Both the incident and reflected spectra are overestimated by a quantity that can exceed 100% for signal-to-noise ratios less than 1. Consequently, estimated reflection coefficients are also overestimated with larger errors occurring when the known reflection is low. Coherence decreases systematically with increasing noise and this trend is used to develop a mathematical function to correct for the observed bias and provide 95% confidence intervals for incident and reflected spectra and reflection coefficients. The correction technique is shown to be very effective in reducing error by up to ~90%. Field data from a natural beach are used to demonstrate the application of these results; corrected values suggest that reflection coefficients are frequently overestimated by over 50%.

Keywords: *Wave reflection, noise, coherence, linear wave theory.*

1. Introduction

Wave reflection is an important process influencing the hydro- and sediment dynamics in front of natural coastlines and man-made coastal structures. Therefore, understanding and accurately predicting the magnitude of wave reflection is essential for estimating potential storm damage, modelling shoreline change, and assessing the reflection performance of marine structures.

Several methods exist to decompose a two-dimensional wave signal propagating over a horizontal bed into its incident and reflected components using cross-shore arrays of spatially separated wave gauges. These methods utilise the phase difference between pairs of wave gauges to provide information on the propagation of the incident and reflected waves. Early methods to calculate wave reflection typically use an array of only two wave gauges (e.g., Goda and Suzuki, 1976; Morden et al., 1976); however, these techniques suffer from singularities at a discrete number of critical frequencies where the distance between the two wave gauges is equal to an integer number of half the corresponding wavelength. To overcome this limitation and estimate wave reflection over a wider frequency range, several newer techniques have been developed that use the wave records from three or more wave gauges (e.g., Battjes et al., 2004; Gaillard et al., 1980; Mansard and Funke, 1980), thus providing a range of wave gauge pairs and separation distances for use in the analysis.

An alternative method of calculating wave reflection is to use a co-located wave gauge and velocity sensor (e.g., Guza and Bowen, 1976; Sheremet et al., 2002), where the direction of wave propagation is estimated using information on the slope of the sea surface provided by the cross-shore current. These methods have the advantage of estimating wave reflection at a singular cross-shore location, whereas the wave reflection estimate from an array method is the average value for the spatial extent of the array, which may be quite large. Additionally, methods that use a co-located wave gauge and velocity sensor are not affected by variations in the bathymetry. However, it is critically important to have the wave gauge and velocity sensor located at the same horizontal location as even a small spatial separation can have important effects on the resulting wave reflection estimates (Huntley et al., 1999). In many cases array methods remain the preferred approach as wave gauges are typically less intrusive to deploy in the field than current sensors and far more economical if wave reflection estimates are required at several cross-shore locations (Hughes, 1993).

Most array methods used to separate incident and reflected waves are designed for two-dimensional waves propagating over a horizontal bed and do not account for the effects of sloping bathymetry such as that of a natural beach. Therefore, depending on the wave conditions and bed slope, errors in the analysis are likely when used in such conditions. Baldock and Simmonds (1999) demonstrated that relatively simple modifications are required to adapt the separation method of Frigaard and Brorsen (1995) to account for shore-normal linear waves propagating over a bed with arbitrary bathymetry. Their analysis showed that neglecting the shoaling effects of waves can lead to large errors in the estimated reflection coefficient (the ratio of reflected to incident wave energy) in cases of low wave reflection. Furthermore, accounting for bathymetry variations was found to be crucial to avoid significant errors (up to 90%) in estimating the incident and reflected wave amplitudes.

An additional source of error that may impact wave reflection estimates, present in both laboratory and field data, is that of noise. Potential sources of signal noise include water surface variability that is unrelated to wave motion, proximity to standing wave nodes, and electronic noise. Using simulated time series of surface elevation and velocity with known true reflection coefficients and added uncorrelated noise, Huntley et al. (1999) show that the presence of noise in the data can introduce a significant positive bias to the reflection coefficients estimated from co-located wave gauge and velocity sensor methods. In an attempt to overcome this, Tatavarti et al. (1988) developed a method using principal component analysis to separate the elevation and velocity time series into orthogonal eigenvector combinations, thus allowing the *correlated* parts of the two time series to be separated from undesired noise. This technique was validated by Huntley et al. (1999) who also demonstrate that the bias in reflection coefficients estimated using other co-located wave gauge and velocity sensor methods can be corrected for by using the estimated reflection coefficient itself and the coherence between the estimated incident and reflected waves. A similar investigation into the effect of noise on wave reflection estimates using array methods is currently lacking.

The aim of this paper is to use simulated time series of water surface elevation to investigate the impact of noise on wave reflection estimates using the array method of Gaillard et al. (1980). A mathematical function is developed to provide a correction for the observed bias in incident and reflected spectra and corresponding reflection coefficients. This function is applied to field data to demonstrate its value. The results presented in this paper are principally applicable to the array method of Gaillard et al. (1980) which was chosen for its relatively simple approach that directly returns incident and reflected spectra from which to assess the noise impact. However, the procedure outlined in the following section could equally be used to assess the impact of noise on other two-dimensional array methods.

2. Methodology

The water surface elevation η at two cross-shore locations, x_1 and x_2, separated by Δx, is given by linear wave theory as

$$\eta(x_1, t) = a_i \cos(\omega t - kx_1 + \phi_i) + a_r \cos(\omega t + kx_1 + \phi_r) \tag{1}$$

$$\eta(x_2, t) = a_i \cos(\omega t - kx_1 - k\Delta x + \phi_i) + a_r \cos(\omega t + kx_1 + k\Delta x + \phi_r) \tag{2}$$

where t is time, a is wave amplitude, ω is wave angular frequency ($2\pi f$, where f is frequency), k is wavenumber ($2\pi/L$, where L is wavelength), ϕ is phase, and subscript i and r denote incident and reflected waves, respectively. The signs of the terms are for an onshore-directed x-axis. Eqs. (1) and (2) show that between cross-shore locations x_1 and x_2, the incident and reflected waves are phase shifted by $-k\Delta x$ and $k\Delta x$, respectively. Eqs. (1) and (2) are used to generate simultaneous time series of water surface elevation at three cross-shore locations on a horizontal bed.

For the purpose of the simulations, wave amplitudes a_i and a_r are independent of frequency and all waves travel at the shallow water wave speed. A range of simulations were performed with incident wave amplitudes between 1 and 10 m, known reflection coefficients between 0 and 1, and with normally distributed, random noise added to the time series at known signal-to-noise ratios (SNR). While the use of constant wave amplitudes and reflection coefficients across all frequencies is not representative of real field data, each frequency provides an independent estimate of the incident and reflected spectra for any particular SNR, wave amplitude and true reflection coefficient. This allows mean values of error, and confidence intervals on these estimates, to be calculated for particular frequency ranges. By running a range of simulations with different wave amplitudes and noise levels, errors and corresponding confidence intervals can be predicted for each frequency bin in a measured spectrum.

Synthetic time series were generated with 4096 data points and a sampling frequency of 4 Hz. Smooth spectral estimates were computed using a 50% overlapping Hanning window, giving a frequency resolution of 0.0039 Hz and 12 degrees of freedom (Nutall, 1971). The spectra are then separated into incident S_i and reflected S_r components using the first order formulae of Gaillard et al. (1980) as

$$S_i(f) = \frac{\bar{S}-\bar{C}+\bar{Q}}{2S_a} \tag{3}$$

$$S_r(f) = \frac{\bar{S}-\bar{C}-\bar{Q}}{2S_a} \tag{4}$$

where

$$\bar{S} = S_1 + S_2 + S_3 \tag{5}$$

$$\bar{C} = C_{21}\cos(k\Delta x_{21}) + C_{31}\cos(k\Delta x_{31}) + C_{32}\cos(k\Delta x_{32}) \tag{6}$$

$$\bar{Q} = Q_{21}\sin(k\Delta x_{21}) + Q_{31}\sin(k\Delta x_{31}) + Q_{32}\sin(k\Delta x_{32}) \tag{7}$$

and

$$S_a = \sin(k\Delta x_{21}) + \sin(k\Delta x_{31}) + \sin(k\Delta x_{32}) \tag{8}$$

where S, C and Q represent the auto-, co-, and quadrature-spectra respectively, Δx is sensor spacing, and subscript numbers denote sensor location (S) or sensor pair (C,Q,Δx). Co- and quadrature-spectra are calculated as the real and imaginary parts of the cross-spectrum, respectively. The incident and reflected spectra are then used to estimate reflection coefficients R by

$$R(f) = \sqrt{\frac{S_r}{S_i}} \tag{9}$$

The purpose of using an array method with three wave gauges is to avoid singularities occurring at a discrete number of critical frequencies. However, gauge triplets must be chosen intelligently with spatial separations that mitigate the coincidence of critical frequencies, otherwise these frequencies will suffer similar effects to those from using a two gauge array. This paper will focus on the frequency range 0.01-0.33 Hz. The low frequency cut-off of 0.01 Hz was chosen to avoid any adverse effects radiating from the singularity that always occurs at 0 Hz, regardless of whether two of three wave gauges are used. The high frequency cut-off of 0.33 Hz was chosen as it coincides with the upper limit of the frequency range commonly used to define ‘short’ waves (e.g., Ruessink, 1998). Furthermore, wave reflection from natural coastlines has been found to be negligible at higher frequencies, particularly on dissipative beaches. The use of this frequency range allows for spectral estimates at 82 discrete frequencies. To avoid the influence of singularities across the entire frequency range of interest, three different array set-ups are used in the simulations to satisfy frequency ranges 0.01-0.05 Hz, 0.05-0.20 Hz, and 0.20-0.33 Hz, respectively. The full range of simulations was performed for each array set-up and spectral estimates for the corresponding three frequency ranges were concatenated providing the full spectrum of interest for each combination of simulation parameters.

3. Results

For each simulation scenario an assessment is made of the accuracy to which the incident and reflected spectra, and corresponding reflection coefficients, are reproduced by the decomposition method of Gaillard et al. (1980). Mean coherence between the three synthetic time series is calculated to investigate the extent to which coherence can be used as a proxy for SNR. By averaging the coherence between the three pairs of time series, fluctuations due to standing wave nodes and antinodes are removed. Throughout this section, target values for incident and reflected spectra and reflection coefficients (i.e., those fixed in the simulations) are denoted by S_i, S_r, and R, respectively. Estimated values are differentiated from target values by the following overbar symbol $\widehat{\ }$, and corrected estimates are represented by an additional subscript c. Error in the estimated values is always positive and is therefore referred to as a bias.

3.1 Noise correction

Fig. 1 shows $\widehat{S_i}$, $\widehat{S_r}$, coherence, and $\hat{R}$ for a wave amplitude of 2 m, R = 0.3, and four different SNRs. With no noise added to the time series, $\widehat{S_i}$ and $\widehat{S_r}$ are estimated accurately with mean values within 3% of their respective target values. $\hat{R}$ is also estimated with reasonable accuracy with a mean value of 0.31. The absence of noise is reflected in a mean coherence value of 0.98. A similar accuracy can be found across all simulations where no noise has been added to the time series, thus providing confidence in the method. For SNR = 2.5, both $\widehat{S_i}$ and $\widehat{S_r}$ are positively biased by 12.2% and 11.7% of S_i respectively, and mean coherence is reduced to 0.72. With $\widehat{S_i}$ and $\widehat{S_r}$ being biased by practically the same amount, the difference in magnitude between $\widehat{S_i}$ and $\widehat{S_r}$ is largely unchanged but becomes smaller relative to the overall magnitudes, thus introducing a positive bias to $\hat{R}$ which has a mean value of 0.43. This is further demonstrated by a SNR of 1.7, which creates a bias in $\widehat{S_i}$ and $\widehat{S_r}$ of 25.8% and

26.3% of the S_i magnitude respectively and increases the mean $\hat{R}$ value to 0.50. A SNR of 0.7 causes $\widehat{S_i}$ and $\widehat{S_r}$ to be biased by 137.4% and 136.0% of S_i respectively which raises the mean $\hat{R}$ from 0.3 to 0.78. However, this is somewhat of an extreme case and coherence values for this simulation are below the 95% confidence threshold and therefore would not be considered significant if found in real data.

Whilst the bias in $\widehat{S_i}$ and $\widehat{S_r}$ is dependant only on the wave amplitude and SNR, the bias in $\hat{R}$ becomes more significant for lower values of true reflection. This is because, while $\widehat{S_i}$ and $\widehat{S_r}$ are biased by the same amount, as the true reflection coefficient decreases from 1 the bias becomes increasingly larger relative to S_r than S_i. For a given SNR, the bias in $\widehat{S_i}$ and $\widehat{S_r}$ increases linearly with increasing wave amplitude. Therefore, normalising by $\widehat{S_i}$ conveniently removes the dependency of bias on wave amplitude, allowing the bias from all simulations to be investigated simultaneously as a function of coherence. This is shown in Fig. 2 where the data have been band-averaged across frequencies thus providing one estimate for each simulation scenario. The frequency smoothing, which increases the degrees of freedom of the estimates from 12 to 984, is performed to provide the best possible estimates from which to predict the expected bias in real data.

The normalised bias $\tilde{\epsilon}$ is shown to decrease exponentially with increasing coherence and an exponential regression function is fit to the data with excellent agreement and a correlation coefficient r^2 of 0.99 (all r^2 values reported herein are significant at the 95% level). This function allows for a prediction of the bias $\hat{\epsilon}$ by

$$\hat{\epsilon} = \widehat{S_i} 1.364 exp^{(-3.705C)} \tag{10}$$

where C is coherence. Corrected incident $\widehat{S_{\iota,c}}$ and reflected $\widehat{S_{r,c}}$ spectra can then be calculated as

$$\widehat{S_{\iota,c}} = \widehat{S_\iota} - \hat{\epsilon} \tag{11}$$

$$\widehat{S_{r,c}} = \widehat{S_r} - \hat{\epsilon} \tag{12}$$

and corrected reflection coefficients $\widehat{R_c}$ as

$$\widehat{R_c} = \sqrt{\frac{\widehat{S_{r,c}}}{\widehat{S_{\iota,c}}}} \tag{13}$$

3.2 Confidence intervals

Reducing the amount of frequency smoothing and degrees of freedom shown in Fig. 2 increases the amount of scatter around the exponential regression function, yet no frequency smoothing and 12 degrees of freedom still yields an r^2 of 0.93. Regardless of the level of frequency smoothing, values of $\tilde{\epsilon}$ remain normally distributed (according to the Shapiro-Wilk normality test) around the exponential regression function. This allows 95% confidence intervals on $\tilde{\epsilon}$ to be calculated for different levels of coherence and degrees of freedom using the t-distribution. These are shown in Fig. 3a for coherence bins of 0.1 and degrees of freedom between 12 and 984 as a result of averaging over particular frequency ranges in the spectrum. Confidence intervals are shown to increase with decreasing coherence and the rate of this increase is steeper for lower degrees of freedom. For example, for 12 degrees of freedom, 95% confidence intervals are ± 0.085 and ± 0.026 for coherence values between 0.5 and 0.6, and 0.9 and 1.0, respectively. Whereas the same confidence intervals for 120 degrees of freedom (equivalent to averaging over the infragravity band) are ± 0.037 and ± 0.010, respectively. Note that confidence intervals are not calculated for coherence bins that include values below the 95% confidence threshold for the respective degrees of freedom. The rate of change in the confidence intervals with coherence is relatively constant and linear regression models yield r^2 between 0.81 and 0.99 for the different degrees of freedom. Figs. 3b and 3c show that the slope m and intercept b from the linear regressions can be predicted accurately (r^2 = 0.97 and 0.98, respectively) using exponential regression functions and the degrees of freedom. This allows 95% confidence intervals on corrected spectra $\Delta\widehat{S_c}$ to be calculated as

$$\Delta\widehat{S_c} = \widehat{S_\iota}\left(\left(-0.141exp^{(-v/69.699)} - 0.015\right)C + \left(0.155exp^{(-v/67.014)} + 0.022\right)\right) \tag{14}$$

where v is degrees of freedom. Using the standard propagation of errors, $\Delta\widehat{S_c}$ is used to calculate 95% confidence intervals on estimated reflection coefficients $\Delta\widehat{R_c}$ as

$$\Delta\widehat{R_c} = \widehat{R_c}0.5\left(\sqrt{\left(\frac{\Delta\widehat{S_c}}{\widehat{S_{r,c}}}\right)^2 + \left(\frac{\Delta\widehat{S_c}}{\widehat{S_{\iota,c}}}\right)^2}\right) \tag{15}$$

3.3 Application to simulated data

The correction technique outlined in Eqs. (10)-(15) is demonstrated in Fig. 4 on simulated data with an incident wave amplitude of 3 m and R = 0.5. For clarity, only incident spectra are shown in Fig. 4a-c. The same bias correction is applied to $\widehat{S_r}$ but percentage deviations of $\widehat{S_{r,c}}$ from the target value are determined by R. With a SNR of 5.0, $\widehat{S_\iota}$ is overestimated by an average of 6.56%, whereas the mean absolute error on $\widehat{S_{\iota,c}}$ is 1.78%. $\widehat{R_c}$ is 0.49 which is an improvement on the $\hat{R}$ estimate of 0.54. Corrected values are similarly accurate for a SNR of 2.5 with a mean error on $\widehat{S_{\iota,c}}$ of 1.83%, compared to 16.11% on $\widehat{S_\iota}$, and a mean $\widehat{R_c}$ 0.50. A SNR of 1.7 causes $\widehat{S_\iota}$ to be overestimated by 31.66%, whilst $\widehat{S_{\iota,c}}$ has a mean error of 2.44%; a decrease in error magnitude of $> 90\%$. Table 1 gives a summary of the errors and 95% confidence intervals depicted in Fig. 4, and for additional SNRs.

SNRs less than 1 (not shown) produce biases of > 100% in $\widehat{S_\iota}$, but the accuracy of the correction technique for these simulations remains in a reasonable range, typically less than 15%, albeit with larger confidence intervals. However, for SNRs less than ~1.5, coherence falls below the 95% confidence threshold for 12 degrees of freedom. Nevertheless, degrees of freedom can be increased by frequency smoothing and/or increasing the number of segments when calculating the spectra, which would reduce the 95% confidence threshold for coherence. Therefore, it is beneficial to know that the correction technique is robust at withstanding extreme levels of noise.

Table 1. Summary of mean errors in estimated and corrected incident spectra and reflection coefficients for a wave amplitude of 3 m, known reflection coefficient of 0.5, and SNRs between infinity and 1. Errors in the estimated and corrected incident spectra, and 95% confidence intervals on corrected incident spectra, are given in terms of percentage of the target value S_i.

SNR	$\bar{C}$	$\epsilon_{\widehat{S_i}}$ %	$\epsilon_{\widehat{S_{i,c}}}$ %	95% $\widehat{S_{i,c}}$ %	$\hat{R}$	$\widehat{R_c}$	95% $\widehat{R_c}$
Inf	0.94	3.52	2.06	± 2.27	0.50	0.47	± 0.03
10.0	0.92	4.41	1.93	± 2.61	0.51	0.47	± 0.03
5.0	0.85	6.56	1.78	± 3.64	0.54	0.49	± 0.04
3.3	0.76	10.52	1.48	± 5.14	0.55	0.49	± 0.05
2.5	0.66	16.11	1.83	± 6.91	0.58	0.50	± 0.07
2	0.56	22.67	2.41	± 8.75	0.61	0.50	± 0.09
1.7	0.49	31.66	2.44	± 10.72	0.65	0.50	± 0.11
1.43	0.42	43.06	3.40	± 12.86	0.68	0.49	± 0.13
1.25	0.37	53.32	3.94	± 14.89	0.71	0.49	± 0.16
1.11	0.33	67.93	4.91	± 17.24	0.74	0.48	± 0.19
1	0.29	82.30	6.03	± 19.62	0.76	0.46	± 0.23

SNR = signal-to-noise ratio, $\bar{C}$ = mean coherence, $\epsilon_{\widehat{S_i}}$ = mean percentage error on the estimated incident spectra, $\epsilon_{\widehat{S_{i,c}}}$ = mean percentage error on the corrected incident spectra, 95% $\widehat{S_{i,c}}$ = mean 95% confidence intervals on corrected incident spectra, $\hat{R}$ = mean estimated reflection coefficient, $\widehat{R_c}$ = mean corrected reflection coefficient, 95% $\widehat{R_c}$ = mean 95% confidence intervals on corrected reflection coefficients.

3.4 Wave angle and directional spreading

The main assumption of array methods for calculating wave reflection is that waves are unidirectional and shore-normal. Additional numerical simulations using oblique waves reveal that the Gaillard et al. (1980) method, and consequently the noise correction, is fairly robust to wave angle with additional errors occurring only when the wave angle exceeds ~40° relative to shore-normal and only becoming significant (> 10%) for angles exceeding ~60°. Nevertheless, these additional errors can be reduced slightly if the Gaillard et al. (1980) method is modified to account for wave refraction effects when applied to field data.

The consequence of directionally spread waves is that the mean coherence between the sensors will decrease without the presence of noise. This could result in an unnecessary correction being applied to the incident and reflected spectra. For this to be significant, the majority of wave energy would need to pass through the array at a highly oblique angle (> 60°). This is unlikely for data collected close to shore or in the study of infragravity waves due to their strong refraction properties. However, one should be aware of the potential consequences of directionally spread waves when applying the noise correction to field data and ensure that the sensor array is aligned as close to the dominant wave direction as possible.

4. Application to field data

To illustrate the application of the results to field data, measurements are used from Perranporth Beach, Cornwall, UK. Perranporth is a macrotidal, dissipative beach composed of medium sand and exposed to both Atlantic swell and locally generated wind-sea. Data were collected during a field experiment in November 2014 using a cross-shore array of 15 pressure transducers logging at 4 Hz. The pressure data were converted to water surface elevation with a depth correction using linear wave theory. Spectra were calculated as with the simulated data outlined in section 2 and separated into incident and reflected components using the Gaillard et al. (1980) array method with modifications for wave shoaling analogous to those implemented by Baldock and Simmonds (1999). The data presented here were collected in the inner surf zone (mean water depth $\bar{h}$ = 1.5 m) during a single tide with an offshore significant wave height H_o of 1.85 m and a spectral peak period T_p of 10.8 s. The focus of the field study was infragravity (0.005-0.05 Hz) waves and so the array set-up was optimised (avoiding singularities) for estimating wave reflection in this frequency range. Therefore, only infragravity data are presented here with a low frequency cut-off of 0.01 Hz as with the simulated data. The analysis of co-located pressure and velocity data from a rig deployed during the field experiment shows that water motion at infragravity frequencies was predominantly cross-shore.

The general trend shown in Fig. 5a is of higher magnitudes of $\widehat{S_\iota}$ and $\widehat{S_r}$ at lower frequencies than higher frequencies with a spectral peak at f = 0.016 Hz; a trend which is preserved in $\widehat{S_{\iota,c}}$ and $\widehat{S_{r,c}}$. The largest correction in terms of spectral density occurs at the spectral peak where $\widehat{S_{\iota,c}}$ and $\widehat{S_{r,c}}$ are reduced by 17.5% and 36.2% of $\widehat{S_\iota}$ and $\widehat{S_r}$, respectively. Larger magnitudes of both $\widehat{S_{\iota,c}}$ and $\widehat{S_{r,c}}$ in the low frequency portion of the infragravity band yield higher $\widehat{R_c}$ estimates with smaller corrections and confidence intervals than higher frequencies. For example, at f = 0.020 Hz, $\widehat{R_c}$ is 0.67 (± 0.06) which is only 0.06 less than $\hat{R}$. In contrast, at f = 0.043 Hz, the $\widehat{R_c}$ value of 0.25 (± 0.15) is significantly less than the $\hat{R}$ estimate of 0.43. The mean infragravity $\hat{R}$ is 0.61 but this is reduced in $\widehat{R_c}$ to 0.54 (± 0.02). Whilst it isn't strictly appropriate to average over the infragravity band given the frequency dependence shown in the data, it does demonstrate the reduction in confidence intervals as a result of more degrees of freedom.

The frequency dependence of infragravity wave reflection, with high levels of reflection limited to low frequencies, is well-documented in the literature (e.g., De Bakker et al., 2014; Guedes et al., 2013). The results presented here suggest that, in failing to correct for bias, $\hat{R}$ values at high infragravity frequencies where wave reflection is low, and indeed at short wave frequencies where reflection tends to be even more minimal, can be overestimated by more than 50%. This is likely to have impacted wave reflection estimates reported previously in the literature where wave gauge arrays have been used.

5. Conclusion

An existing two-dimensional method for separating incident and reflected wave spectra using an array of wave gauges is investigated for its sensitivity to random noise. Linear wave theory is used to generate simulated time series of water surface elevation at three cross-shore locations with varying wave amplitudes, known reflection coefficients, and signal-to-noise ratios. Both the incident and reflected spectra are shown to be positively biased by noise and in turn this causes reflection coefficients to be overestimated. The magnitude of the bias is found to be dependent on wave amplitude, but not on the true reflection coefficient. Utilizing the systematic change in coherence with noise, a relatively simple and easy to apply method to correct for the observed bias is developed. This correction technique can be applied across all frequencies and is considerably accurate with residual error on corrected incident spectra estimates typically in the region of 2-3% for significant coherence levels; an improvement of over 90% for low signal-to-noise ratios. Applying the correction to field data implies that reflection coefficients can be overestimated by at least 50%. Consequently, if accurate estimates of incident and reflected spectra and corresponding reflection coefficients are required, then potential signal noise must be acknowledged and accounted for.

Acknowledgements

The authors would like to thank Sam Prodger, Kit Stokes, Tim Poate, Erwin Bergsma, Olivier Burvingt, and Peter Ganderton for their assistance during the Perranporth field experiment. The comments and suggestions made by two reviewers helped improved the clarity of the manuscript.

References

Baldock, T.E., Simmonds, D.J., 1999. Separation of incident and reflected waves over sloping bathymetry. Coast. Eng. 38, 167-176. doi:10.1016/S0378-3839(99)00046-0

Battjes, J.A., Bakkenes, H.J., Janssen, T.T., van Dongeren, A.R., 2004. Shoaling of subharmonic gravity waves. J. Geophys. Res. 109, C02009. http://dx.doi.org/10.1029/2003JC001863

De Bakker, A.T.M., Tissier, M.F.S., Ruessink, B.G., 2014. Shoreline dissipation of infragravity waves. Cont. Shelf Res. 72, 73-82. doi:10.1016/j.csr.2013.11.013

Frigaard, P., Brorsen, M., 1995. A time-domain method for separating incident and reflected irregular waves. Coast. Eng. 24, 205-215. doi:10.1016/0378-3839(94)00035-V

Gaillard, P., Gauthier, M., Holly, F., 1980. Method of analysis of random wave experiments with reflecting coastal structures. Proceedings of the 17th Conference on Coastal Engineering. ASCE, New York.

Goda, Y., Suzuki, Y., 1976. Estimation of incident and reflected waves in random wave experiments. Proceedings of the 15th Conference on Coastal Engineering. ASCE, New York.

Guedes, R.M.C., Bryan, K.R., Coco, G., 2013. Observations of wave energy fluxes and swash motions on a low-sloping, dissipative beach. J. Geophys. Res. 118, 3651-3669. 10.1002/jgrc.20267

Guza, R.T., Bowen, A.J., 1976. Resonant interactions for waves breaking on a beach. Proceedings of the 15th Conference on Coastal Engineering. ASCE, New York.

Hughes, S.A., 1993. Physical models and laboratory techniques in coastal engineering. World Scientific, Singapore.

Huntley, D.A., Simmonds, D., Tatavarti, R., 1999. Use of collocated sensors to measure coastal wave reflection. J. Waterw. Port Coast. Ocean Eng. 125, 46-52. http://dx.doi.org/10.1061/(ASCE)0733-950X(1999)125:1(46)

Mansard, E.P.D., Funke, E.R., 1980. The measurement of incident and reflected spectra using a least squares method. Proceedings of the 17th Conference on Coastal Engineering. ASCE, New York.

Morden, D.B., Richey, E.P., Christensen, D.R., 1976. Decomposition of co-existing random wave energy. Proceedings of the 15th Conference on Coastal Engineering. ASCE, New York.

Nutall, A.H., 1971. Spectral estimation by means of overlapped FFT processing of windowed data. Report No. 4169. Naval Underwater Systems Center (NUSC), New London, Connecticut.

Ruessink, B.G., 1998. The temporal and spatial variability of infragravity energy in a barred nearshore zone. Cont. Shelf Res. 18, 585-605. doi:10.1016/S0278-4343(97)00055-1

Sheremet, A., Guza, R.T., Elgar, S., Herbers, T.H.C., 2002. Observations of nearshore infragravity waves: Seaward and shoreward propagating components. J. Geophys. Res. 107, 3095. http://dx.doi.org/10.1029/2001JC000970

Shumway, R.H., Stoffer, D.S., 2000. Time Series Analysis and Its Applications. Springer, New York.

Tatavarti, R.V.S.N., Huntley, D.A., Bowen, A.J., 1988. Incoming and outgoing wave interactions on beaches. Proceedings of the 21st Conference on Coastal Engineering. ASCE, New York.

Figure captions

Fig. 1. Estimated incident $\widehat{S_\iota}$ and reflected $\widehat{S_r}$ spectra (a-d), coherence (e-h), and estimated reflection coefficients $\hat{R}$ (i-l) for SNR = Inf, 2.5, 1.7, and 0.7 as stated on the figure. Dashed lines in a-d are the target incident S_i and reflected S_r spectra. Red dashed line in e-h is the 95% confidence threshold on coherence of 0.45 for 12 degrees of freedom (Shumway and Stoffer, 2000). Red dashed line in (i-l) is the target reflection coefficient R of 0.3. Wave amplitude is 2 m.

Fig. 2. Normalised bias $\tilde{\epsilon}$ ($\epsilon/\widehat{S_\iota}$, where ϵ is bias) versus coherence for all wave amplitudes, true reflection coefficients, and SNRs. Data have been smoothed providing one estimate per simulation and 984 degrees of freedom. Solid red line is an exponential regression function with coefficients and accuracy given on the figure.

Fig. 3. (a) 95% confidence intervals on normalised bias $\Delta\tilde{\epsilon}$ for various degrees of freedom versus coherence. Solid lines are linear regression lines fit to the data of the corresponding colour. (b) Slopes m and (c) intercepts b from the linear regression lines shown in (a) versus degrees of freedom. Solid red lines in (b) and (c) are exponential regression functions with coefficients and accuracy given on the figure.

Fig. 4. (a-c) Deviation (%) of uncorrected $\widehat{S_\iota}$ and corrected $\widehat{S_{\iota,c}}$ incident spectra from the target value S_i. Shaded areas are 95% confidence intervals on $\widehat{S_{\iota,c}}$. (d-f) Coherence, and (g-i) uncorrected $\hat{R}$ and corrected $\widehat{R_c}$ reflection coefficients. Shaded areas are 95% confidence intervals on $\widehat{R_c}$. SNRs are 5.0, 2.5, and 1.7 as stated on the figure. Red dashed line in (d-f) is the 95% confidence threshold on coherence of 0.45 for 12 degrees of freedom (Shumway and

Stoffer, 2000). Red dashed line in (g-i) is the target reflection coefficient R of 0.5. Wave amplitude is 3 m.

Fig. 5. Data from the inner surf zone of Perranporth Beach, UK (H_o = 1.85 m, T_p = 10.8 s). (a) Corrected incident $\widehat{S_{\iota,c}}$ and reflected $\widehat{S_{r,c}}$ spectra, and uncorrected incident $\widehat{S_\iota}$ and reflected $\widehat{S_r}$ spectra. Shaded areas are 95% confidence intervals on $\widehat{S_{\iota,c}}$ and $\widehat{S_{r,c}}$. (b) Coherence and (c) corrected $\widehat{R_c}$ and uncorrected $\hat{R}$ estimated reflection coefficients. Shaded areas are 95% confidence intervals on $\widehat{R_c}$. Red dashed line in (b) is the 95% confidence threshold on coherence of 0.45 for 12 degrees of freedom (Shumway and Stoffer, 2000).

Figure 1

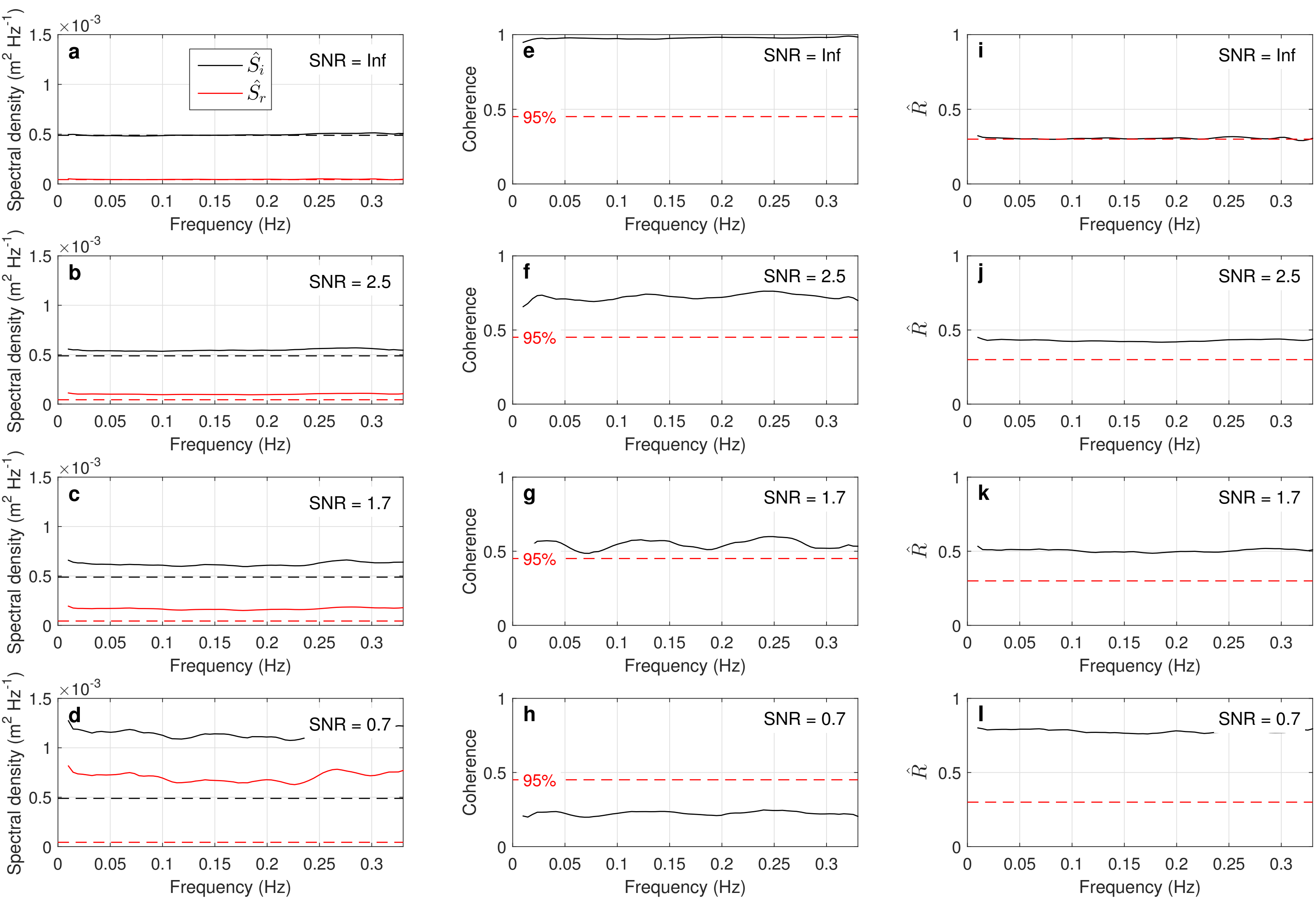

a
b
c
d
e
f
g
h
i
j
k
l
SNR = Inf
SNR = 2.5
SNR = 1.7
SNR = 0.7
$\hat{S}_i$
$\hat{S}_r$
95%
Spectral density (m^2 Hz^{-1})
Coherence
$\hat{R}$
Frequency (Hz)
$\times 10^{-3}$

Figure 2

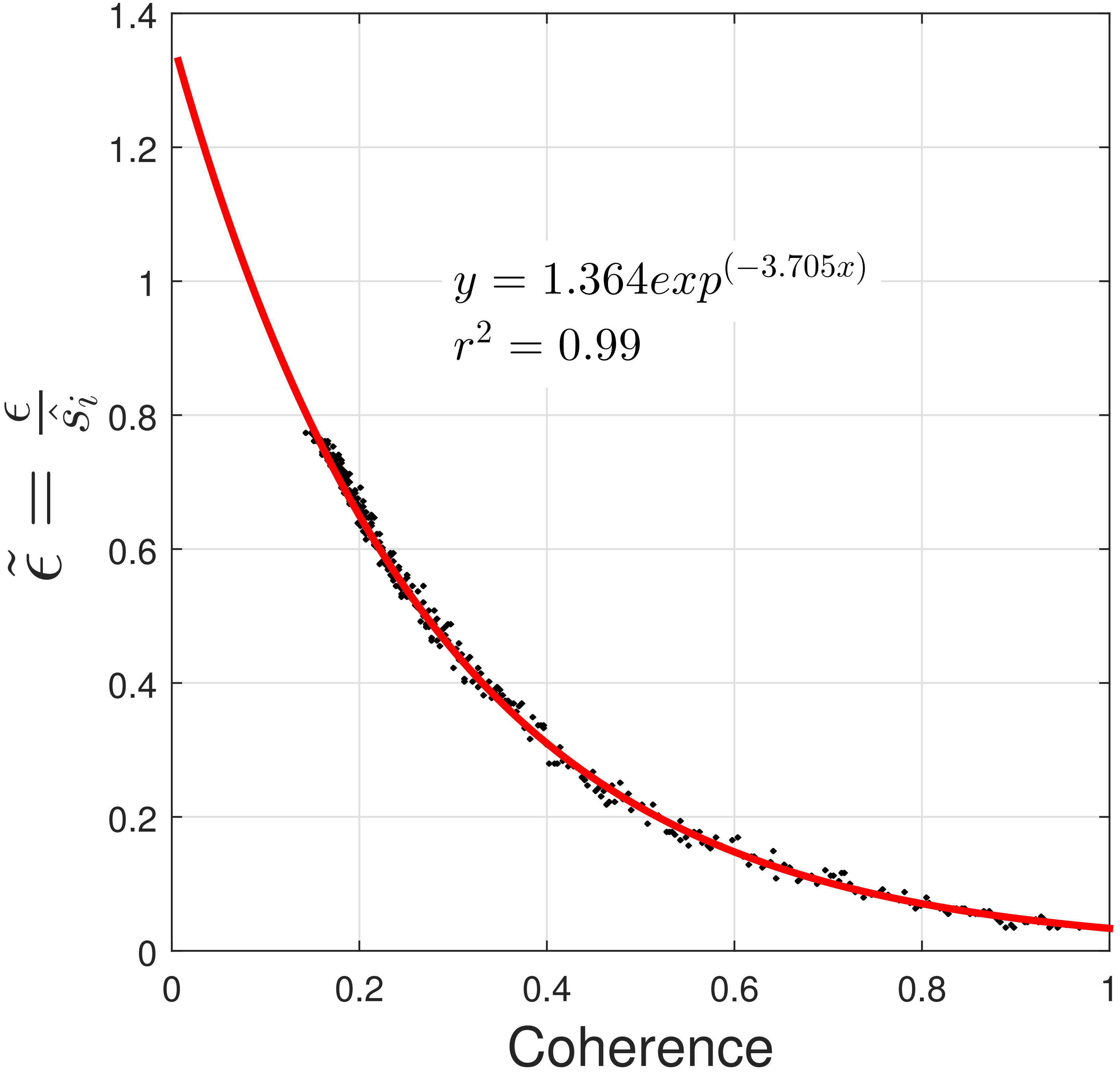

$y = 1.364exp^{(-3.705x)}$
$r^2 = 0.99$
$\tilde{\epsilon} = \frac{\epsilon}{\hat{s}_i}$
Coherence
0
0.2
0.4
0.6
0.8
1
1.2
1.4

Figure 3

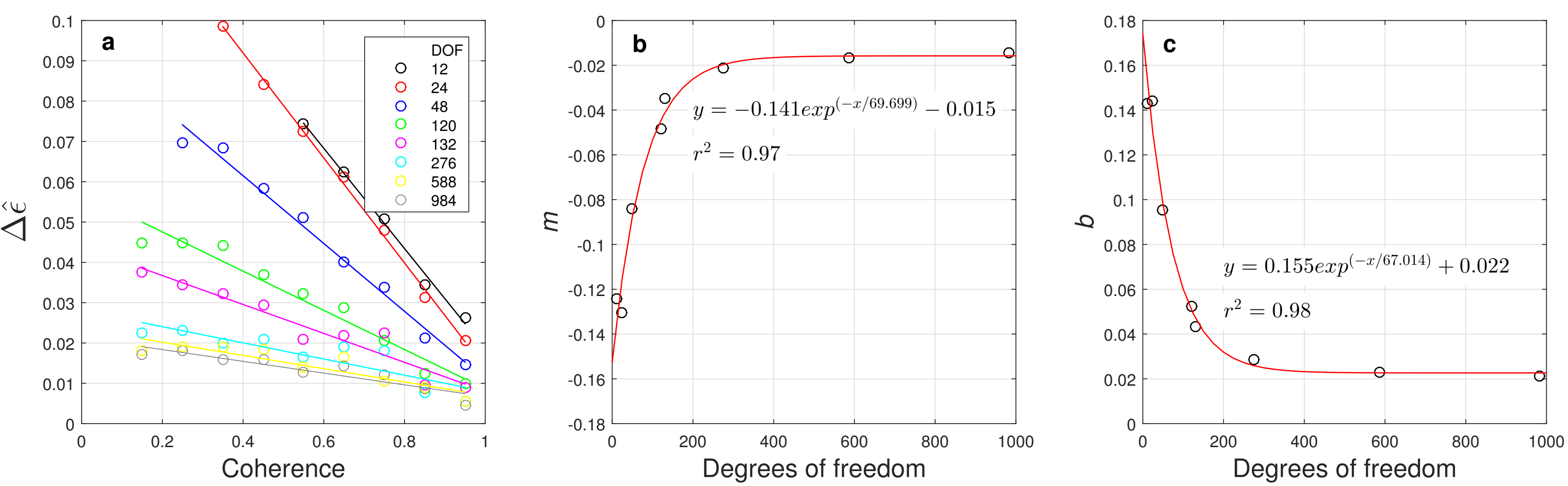

a
DOF
12
24
48
120
132
276
588
984
$\Delta\hat{\epsilon}$
Coherence
b
$y = -0.141exp^{(-x/69.699)} - 0.015$
$r^2 = 0.97$
m
Degrees of freedom
c
$y = 0.155exp^{(-x/67.014)} + 0.022$
$r^2 = 0.98$
b
Degrees of freedom

Figure 4

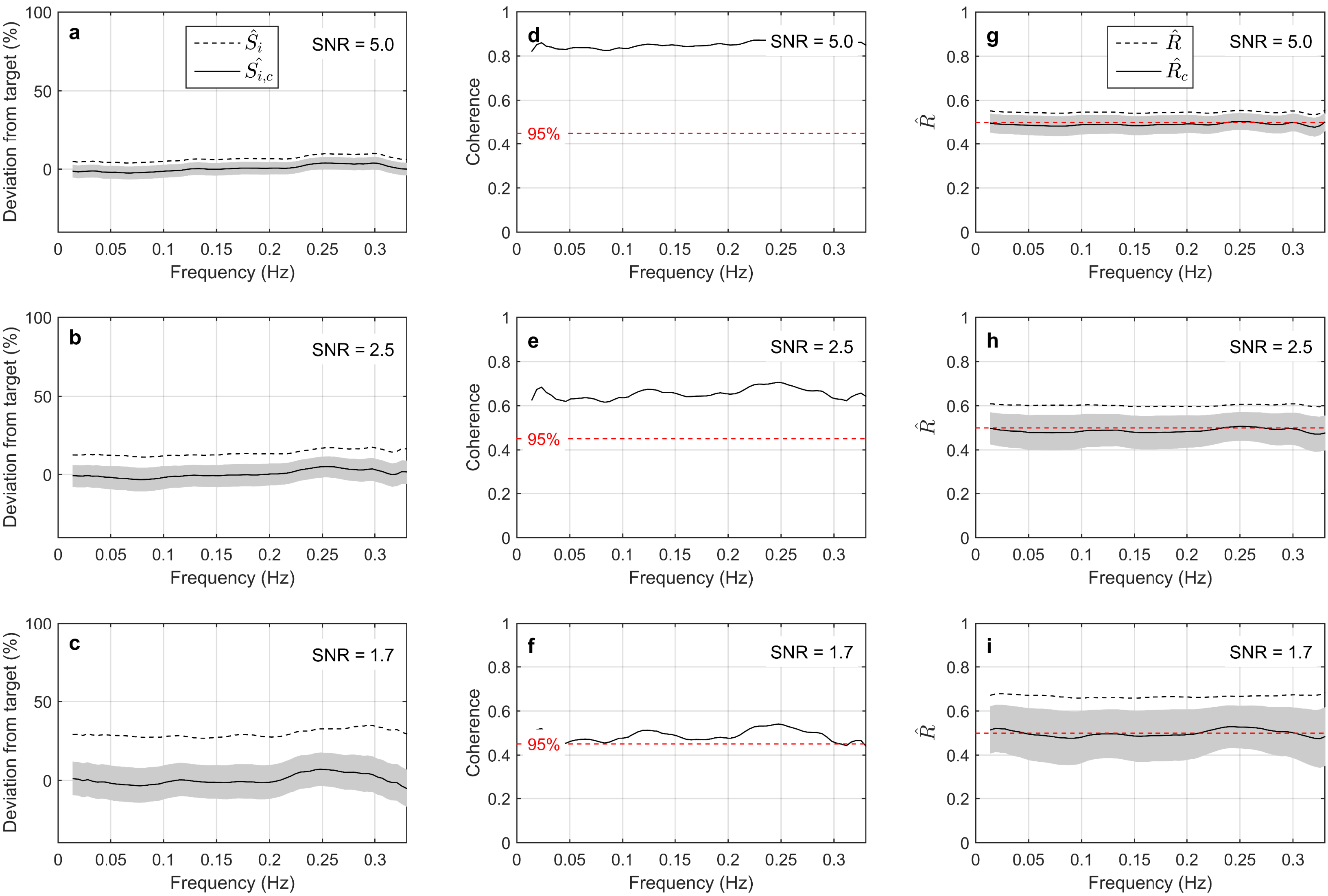

a
b
c
d
e
f
g
h
i
SNR = 5.0
SNR = 2.5
SNR = 1.7
$\hat{S}_i$
$\hat{S_{i,c}}$
$\hat{R}$
$\hat{R}_c$
Deviation from target (%)
Coherence
95%
Frequency (Hz)

Figure 5

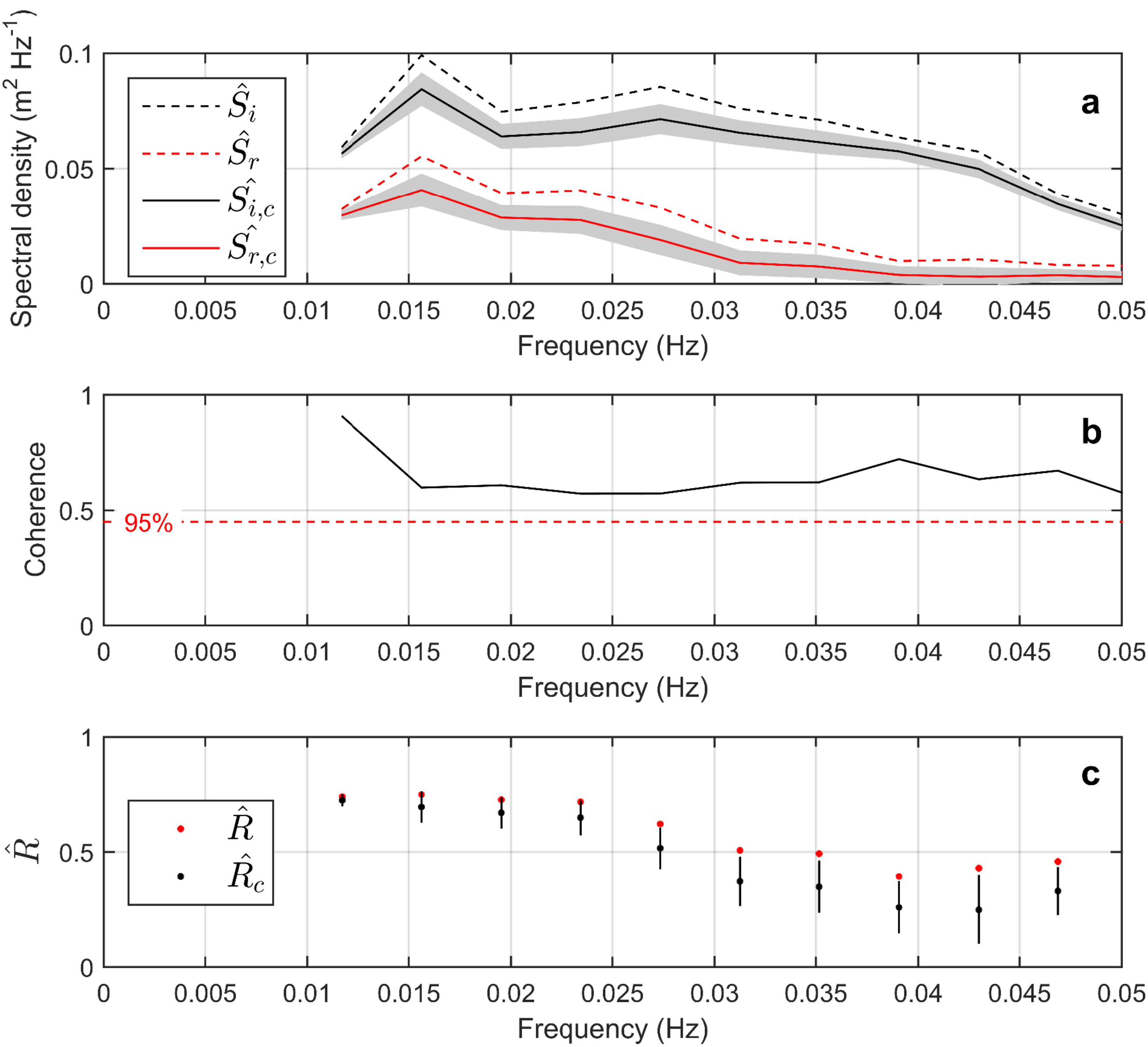

Spectral density (m^2 Hz^{-1})
Frequency (Hz)
$\hat{S}_i$
$\hat{S}_r$
$\hat{S_{i,c}}$
$\hat{S_{r,c}}$
a
Coherence
95%
b
$\hat{R}$
$\hat{R}_c$
c